Improved 3D imaging of phase shifting digital holographic microscope by compensation for wavefront distortion

Improved 3D imaging of phase shifting digital holographic microscope by compensation for wavefront distortion

V Cazac[1,2]

[1]Institute of Applied Physics of Moldova, Chisinau, Moldova
[2]Computing Sciences Unit, Tampere University, Tampere, Finland

Abstract. This paper is focused on improving the performance of quantitative phase imaging via phase-shifting digital holographic microscope. The development of the interferometric techniques is important for technology and biomedicine, since the surface and structure of samples can be monitored in real-time by non-destructive investigations. The novelty of the optical arrangement is that in the reference beam of the digital holographic microscope a liquid crystal variable retarder is introduced. Thus, it became possible to actively control the polarization state of light for realizing the necessary phase-shifts. In addition, a spatial light modulator is integrated in the optical setup to produce computer-controlled compensation of the spatial distortion. An ad hoc hologram processing technique was developed to execute the numerical correction of the physical phase-shifting errors. Topographical investigations of phase masks recorded on carbazol-based azopolymers provided the experimental testing of the achieved accuracy in phase reconstruction.

1. Introduction

Nowadays, various interferometric imaging techniques (IIT) as differential interference contrast, Fourier phase microscopy, Hilbert phase microscopy, and digital holographic microscopy (DHM) have been developed to obtain full field, absolute and quantitative phase imaging, especially for life sciences and biomedical applications [1-4]. The major advantage of IIT compared to conventional phase microscopy systems (i.e. phase contrast microscopy) is the real-time and non-destructive imaging performance that employs the principle of interferometry to measure the optical field [5]. Interferometric approach is remarkable since it enables recording of complex object wavefront named hologram that encodes phase and amplitude information of the specimen. The hologram is obtained by interference of the wave that passes through the object under study and the reference wave set under an angle in off-axis setup, or in-line in case of the phase-shifting configuration. The delivered quantitative phase data make interferometric systems the key instrument for 3D investigation of transparent samples [6,7]. In addition, digitalization of the interferograms open the access to the numerical processing of the complex object wavefront for revealing the phase, amplitude and 3D map of the sample. Nevertheless, a major disadvantage has been identified in accurate measurement of specimen phase, namely wavefront aberrations introduced by the optical components of the setup (microscope objective, lenses, etc.), which may corrupt the contrast, resolution and sensitivity of IIT [8].

Existing solutions for the phase reconstruction improvement of IIT result from the dependence of the resolving power on the wavelength and numerical aperture (NA) of the microscope objective (MO) described by the Abbe criterion. The limited NA of the microscope restricts the spatial-frequency content of the object arrived at the image plane. Previous attempts to apply a short-wavelength laser (UV range) proved to be destructive and phototoxic for investigation of biological objects [9]. Other works demonstrated enlarged spatial frequency coverage by creating a synthetic numerical aperture [10,11]. For this purpose, M. Paturzo and P. Ferraro introduced a diffraction grating between the object and the CCD sensor in the lensless DHM setup [12]. Later, successful integration of spatial light modulators (SLMs) in the DHM optical setup permitted fast and precise operation of the object wavefront for generating the desired structured patterns [13-16].

The aim of this work is to achieve compensation of object wavefront deviations in a phase-shifting (P-S) DHM arrangement. For this purpose, digital modulation of light in the object beam is operated by the spatial light modulator (SLM). The use of the digital approach to wavefront modulation provided by SLM offered several advantages compared to beam shaping by a phase mask recorded on a thin film. First, it permits accurate control and strikethrough alignment of the required phase modulation. Second, it gives quick access to a variety of pattern parameters and shapes that are difficult, or sometimes impossible, to inscribe on a physical diffraction grating. The optimal modulation shape of the object wave is determined by testing three types of phase masks (sinusoidal and blazed diffraction gratings, and binary Fresnel lens) via computer simulations. The phase-shifts in the reference arm of the set-up are computer-controlled by the liquid crystal variable retarder (LCVR). The utilisation of LCVR allows to overcome the probable P-S errors present in the typical P-S scheme resulted from mechanical movements, made by a piezoelectric transducer that may suffer from nonlinearity, hysteresis, and sensibility to temperature [8-10]. In addition, the automatic control of the LCVR permits the hologram registration in a very short period of time (milliseconds). This overcomes the temperature instability and reduces the sequential noise usually affecting the image quality.

2. Simulation results

Simulation parameters correspond to the values of the parameters of the optical setup built in the laboratory: a laser source CW DPSS single mode with the wavelength of 532 nm, barbara test image as test object figure 1(a), a sinusoidal figure 1(b) and blazed diffraction grating figure 1(c) and a Fresnel zone lens figure 1(d) were examined as object wavefront modulation phase-masks, the SLM with the pixel size of 34μm, and the CMOS sensor with the pixel size of 3.45 μm and maximum resolution of 2448 × 2048. The distance between the phase masks (imaged on SLM) and the object was set x=3 cm. At this distance, the diffraction orders are not superimposed. The optimal phase-masks parameters are determined by varying the diffraction gratings period P and angle α in relation to the optical axis of the imaging system and the number of concentric rings in the experiment with a Fresnel zone lens. For matching the real laboratory conditions Poisson and Gauss distribution noise was introduced in the setup.

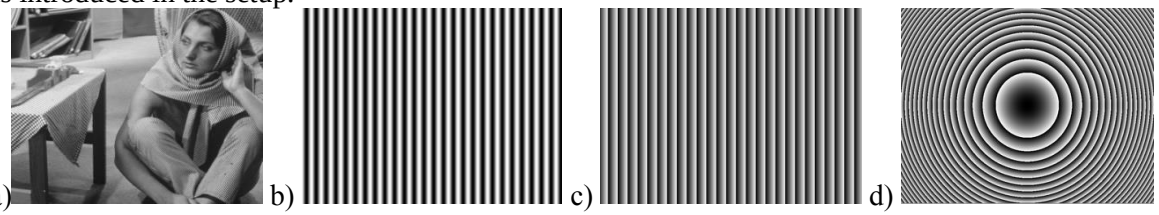

Figure 1. (a) Barbara test image, (b) sinusoidal diffraction grating, (c) blazed diffraction grating and (d) Fresnel zone lens phase-mask.

The accuracy of the phase reconstruction is evaluated by the relative root mean square error (RRMSE):

$$\mathrm{RRMSE} = \frac{\|\varphi_0 - \widehat{\varphi_0}\|_F}{\|\varphi_0\|_F} \quad (1)$$

where φ_0 and $\widehat{\varphi_0}$ are the phases of initial and reconstructed object, and $\|\cdot\|_F$ is the Frobenius norm. When RRMSE<0.11 the reconstruction is considered to be successful [17].

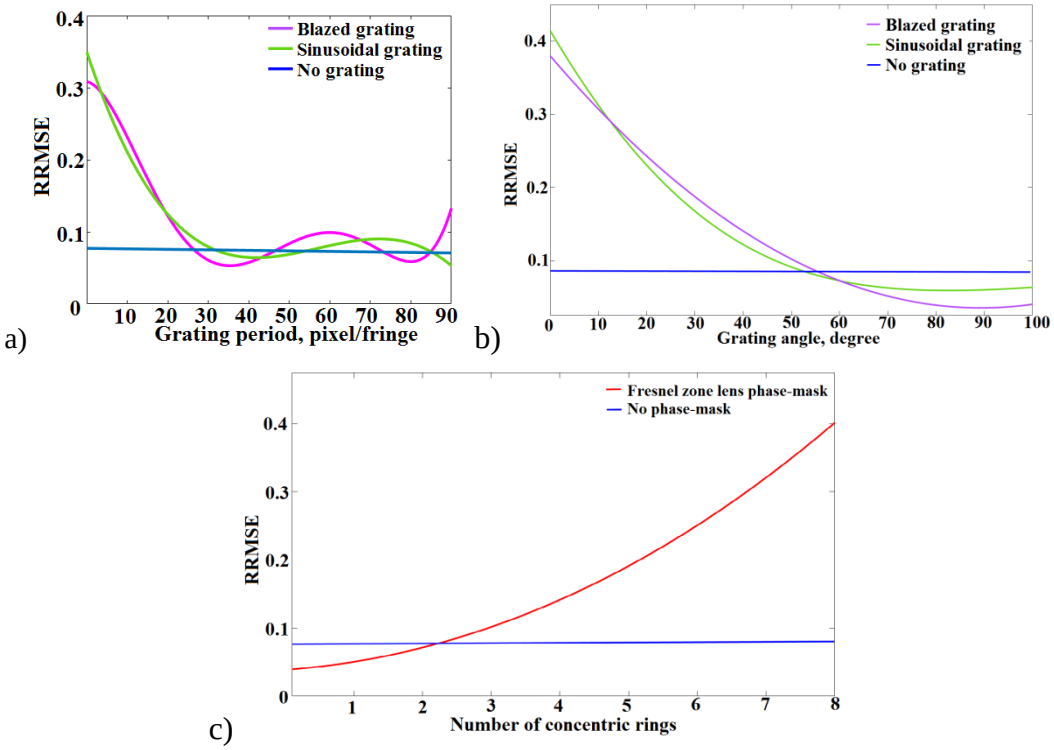

Figure 2. (a) RMSE dependance on the sinusoidal and blazed gratings period; (b) RMSE dependance on the sinusoidal and blazed gratings angle in relation to the optical axis of the imaging system; (c) RMSE dependance on the number of concentrinc rings of Fresnel zone lens.

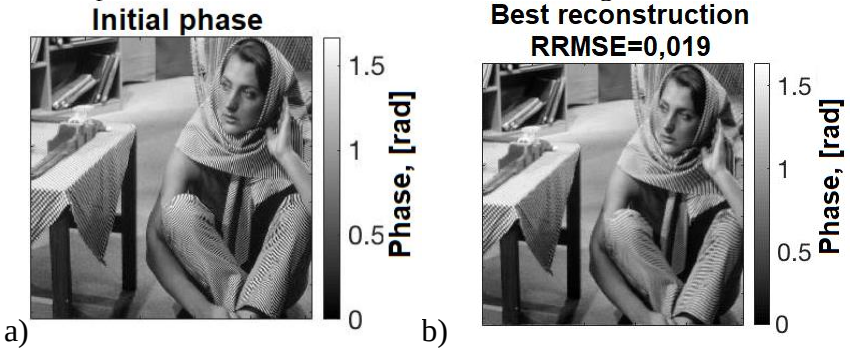

Figure 3. Illustration of (a) initial phase and b. the best phase reconstruction of barbara test image resulted from the modulation of the object wavefront by a blazed grating with the period P=90 Pixel/fringe and angle α=900, with respect to the optical axis of the DHM.

Through the simulation experiments the optimal shaping of the object wavefront was determined. figure 2(a) shows that the best reconstruction can be obtained for the blazed grating when the grating period is equal 35 and 80 pixels/fringe. At these values, the phase reconstruction quality is improved if compared to the experiment without the wavefront modulation by the blazed grating. From figure 2(b) it can be determined that the optimal angle is $\alpha=90^0$ with respect to the optical axis of the DHM. Also, better reconstruction results are obtained when α is in the range of $60\text{-}90^0$. The relation between RRMSE and number of concentric rings of the Fresnel zone lens is inversly proportional. The most accurate results are obtained in the experiment with a single ring. To sum up, the computational simulation results suggest that application of a blazed wavefront provide the best compensation for the

wavefront deviations in the modeled setup. Therefore, with regards to the practical experiments described in this paper a blazed grating with the determined optimal parameters was set on the SLM display.

3. Physical Experiments

The setup of the proposed P-S interferometer is shown in figure 4. This configuration offers the advantage of simultaneously capturing 3D information about the sample under study. The lateral resolving power of the optical system is diffraction-limited according to Abbe criterion.

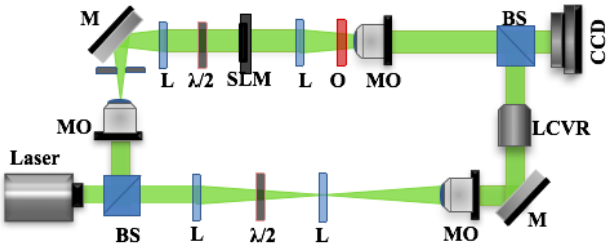

Figure 4. DHM setup: TEM00 DPSS laser (λ=532nm, 100 mW), BS-beam splitter, λ/2- half-wave plates, M-mirror, MO-microscope objective x20, NA=0.40, SLM- HoloEye LC2002 spatial light modulator, O-object, BS-beam splitter, L-lens, CMOS- "Imaging source DMK33UX264" camera - resolution 2,448×2,048 (5 MP), LCVR- "Meadowlark optics" liquid crystal variable retarder LCVR-100.

In the experiment, the laser beam is divided by a beam-splitter into the reference wave with the intensity I_{Rw} and the object signal with the intensity I_{Ow}. Since the LCVR and SLM exhibit birefringence properties, a half-wave plate is introduced in each arm to ensure similar polarization directions of both beams and so to increase the contrast of interference pattern. For precise phase control, these devices were preliminary calibrated. To produce specific phase shifts equal to $\varphi_1 = 0$, $\varphi_2 = \pi/2$, $\varphi_3 = \pi$, $\varphi_4 = 3\pi/2$ a linear approximation of the LCVR phase shift in the region 2-3.2V of the applied voltages was built to exclude their temperature dependence. It was determined that the four required phase changes correspond to the voltages V_1 = 2.02V, V_2 = 2.39V, V_3 = 2.76V, V_4 = 3.14V, respectively.

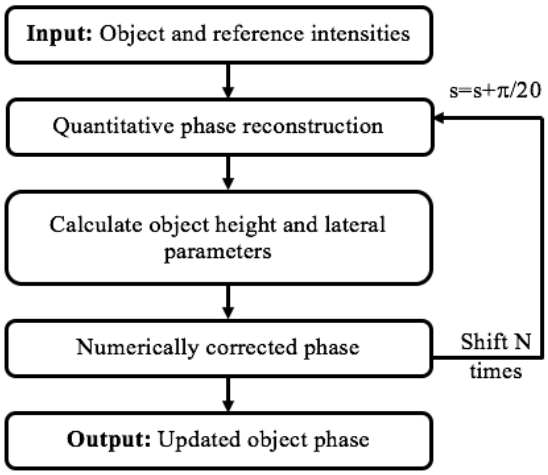

Figure 5. Flowchart of reconstruction method from phase-shifting holograms.

The digital hologram recorded by the CMOS camera is a result of the interference of the object beam $I_{Ow} = A_O \exp(i\Phi_O)$ and reference beam $I_{Rw} = A_R \exp(i\Phi_R + \varphi_N)$, whose intensity is given as

$$I_H = |I_{Ow} + I_{Rw}|^2 \quad (2)$$

where, A_O, A_R and Φ_O, Φ_R are the amplitudes and the phases of the object and reference waves, respectively, and φ_N represents the phase changes N=1, 2, 3, 4 in the reference arm created by the LCVR. The object phase can be quantitatively reconstructed from the four recorded interferograms using the formula

$$\Delta\Phi = \tan^{-1}\left[\frac{I_1 - I_3}{I_2 - I_4}\right] \quad (3)$$

where, I_1, I_2, I_3, I_4 are the four recorded intensities under corresponding phase shifts. Fast hologram acquisition (within 30 milliseconds) was performed for ensuring real time phase imaging.

The numerical reconstruction algorithm illustrated in figure 5 executes the correction of the phase shifts in case of distorted tilt produced by LCVR. This step is important when the appropriate laboratory conditions (temperature, excessive building vibrations, etc.) cannot be maintained. A small phase shift is added during the phase reconstruction stage until the object phase is successfully revealed.

4. Results and Discussions

The feasibility of the developed system was tested on a phase mask recorded on the thin film of azopolymer - polyepoxypropil carbazole: disperse orange. Figure 6. and figure 7. illustrate the 3D topography of the reconstructed phase and the surface cross-section of the phase mask in the experiment where the phase imaging is made in preliminary P-S DHM configuration and in the case of corrected object wave performed via SLM, respectively. The measurements effectuated by the P-S DHM indicate the depth of the mask relief that equals to 400 nm and the close to rectangular shape of the surface profile. The obtained relief depth corresponds to the theoretical data about the phase mask. By analyzing both initial and after phase correction experiments (figure 6 and figure 7, respectively), we observe a better accuracy of recovered phase in the second scenario, where the phase image is sharper without using additional noise filtering. The improved imaging system resolves the side peaks that have appeared in the areas of depth minima figure 6.

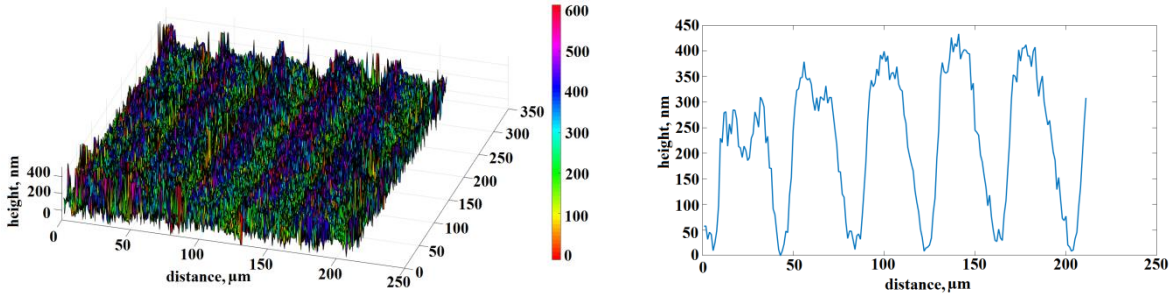

a) b)

Figure 6. Initial results- (a) 3D topography, (b) Cross-section of the phase mask recorded on carbasol-based azopolimer.

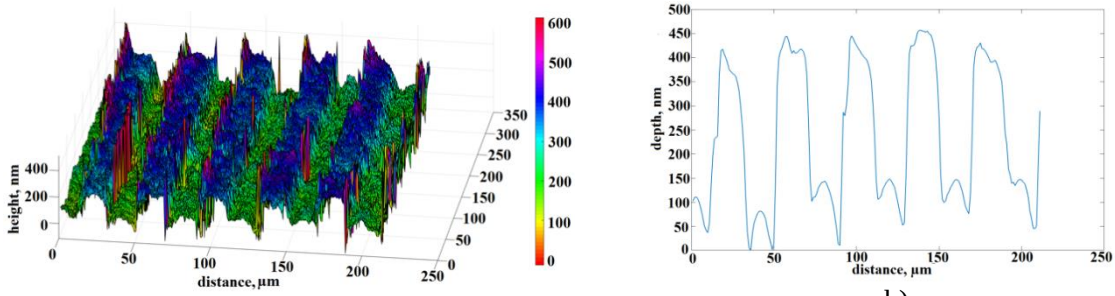

a) b)

Figure 7. Performance results of the experiment including the compensation stage implemended by the SLM- (a) 3D topography, (b) Cross-section of the phase mask recorded on carbasol-based azopolimer.

These peaks are related to the shape of the dual-range diffraction grating recorded on the polymer material. By this way, for validating the simulation results the designed optical system was tested on previously unknown objects, and new features of recorded gratings were noticed.

5. Conclusion

In summary, this work proves the feasibility of the modified P-S DHM technique as a tool for quantitative phase measurements of phase objects. In particular, we have demonstrated that by utilizing liquid crystal devices (SLM and LCVR) in the interferometric setup we can control the precision of the phase reconstruction. Due to the independent phase control of the object wave and the reference wave, significantly improved 3D phase images are obtained. In addition, the proposed method involves the compensation of the system noise (aberration of optical components, shot noise of the camera and SLM), and the environmental noise, which are usually present even in laboratory conditions.

6. Acknowledgment

The author of this paper is thankful to the Laboratory for Materials of Photonics and Photovoltaics from the Institute of Applied Physics, especially to Elena Achimova, Vladimir Katkovnik and Vladimir Abashkin who provided expertise that greatly inspired the work, as well as Alexander Prisacar and Constantin Loshmanskii for sharing the phase masks recorded on the carbazol-based azopolymer as test objects.

This work was partially supported by the bilateral project No. 19.80013.50.07.04A / BL.

7. References

[1] Shribak M 2019 *Microsc. Microanal.* **25** 1234-1235.
[2] Popescu G, Deflores L P, Vaughan J C, Badizadegan K, Iwai H, Dasari R R and Feld M S 2004 *Opt. Lett.* **29** 2503-2505.
[3] Ikeda T, Dasari R G and Feld M S 2005 *Opt. Lett.* **30** 1165-1167.
[4] Mir M, Bharduri B, Wang R, Zhu R and Popescu G 2012 *Progress in Optics* **57** 134-179.
[5] Cazac V, Meshalkin A, Abashkin V, Achimova A, Katkovnik V, Shevkunov I, Claus D and Pedrini G 2018 *Appl. Opt*. **57** 507-513.
[6] Osten W, Faridian A, Gao P, Körner K,Naik D, Pedrini G, Singh A K, Takeda M and Wilke M 2014 *App. Opt.* **53** 44-63.
[7] Achimova E, Abaskin V, Claus D, Pedrini G, Shevkunov I and Katkovnik V 2018 Noise minimised high resolution digital holographic microscopy applied to surface topography *Computer Optics* **42(2)** 267-272 DOI: 10.18287/2412-6179-2018-42-2-267-272.
[8] KyeoReh L, Kyoohyun K, Jaehwang J, JiHan H, Sangyeon C, Sangyun L, Gyuyoung C, YoungJu Jo, Hyunjoo P and Yong Keun P 2013 *Sensors* **13** 4170-4191.
[9] Faridian A, Hopp D, Pedrini G, Eigenthaler U, Hirscher M and Osten W 2010 *Opt. Express* **18** 14159-14164.
[10] Gustafsson M G L 2000 *J. Microsc*. **198** 82-87.
[11] Granero L, Micó V, Zalevsky Z and García J 2009 *Opt. Express* **17** 15008-15022.
[12] Paturzo M and Ferraro P 2009 *Opt. Lett*. **34** 3650-3652.
[13] O'Connor T, Doblas A and Javidi B 2019 *Opt. Lett.* **44(9)** 2326-2329.
[14] Zheng J, Gao P, Yao B, Ye T, Lei M, Min J, Dan D, Yang Y and Yan S 2014 *Photon. Res*. **2** 87.
[15] Mosk A P, Lagendijk A, Lerosey G and Fink M 2012 *Nat. Photonics* **6** 283-292.
[16] Jang J, Lim J, Yu H, Choi H, Ha J, Park J, Oh W, Jang W, Lee S and Park Y 2013 *Opt. Express* **21** 2890-2902.
[17] Kocsis P, Shevkunov I, Katkovnik V and Egiazarian K 2020 *Opt. Express* **28** 4625-4637.